S-Band Smallsat InSAR Constellation for Surface Deformation Science

Anthony Freeman
Jet Propulsion Laboratory
California Institute of Technology
Pasadena, CA, USA
anthony.freeman@jpl.nasa.gov

Nacer Chahat
Jet Propulsion Laboratory
California Institute of Technology
Pasadena, CA, USA

***Abstract*—Surface deformation studies using repeat-pass interferometric SAR have evolved into a powerful tool for geophysicists studying earthquake fault zones, volcanoes, ice sheet motion, and subterranean aquifers. Longer wavelengths (S-Band and L-Band) are preferred because they do not decorrelate as quickly as shorter wavelengths. Rapid revisit (1-3 days) is preferred because it allows the study of these phenomena at the timescales at which they commonly occur. Global access on such timescales is also required. Vector surface deformation measurements, taken from more than one direction, are a desired feature.**

This paper describes the conceptual architecture of a longer wavelength, Smallsat SAR constellation of up to 12 satellites for rapid revisit surface deformation studies. The key to making such a constellation affordable is to lower launch costs, spacecraft costs, and instrument (SAR) costs. The first two objectives can be achieved using an ESPA-ring class, or Smallsat, spacecraft. The third objective requires a SAR instrument sized to fit the mass and volume constraints imposed by such a spacecraft. Current state-of-the-art in miniaturization of electronics means that the radar transmit, receive and data handling functions can easily be implemented in a compact, low mass solution. The most significant challenge in designing a SAR to fit the Smallsat paradigm is in the dimensions of the antenna.

The antenna sizing problem is addressed by adopting a smaller antenna than allowed by conventional SAR design rules. The baseline antenna design is simple, requiring no electronic beam-steering or beam-forming capability. Both reflectarray and microstrip patch antenna solutions are considered. The antenna structure is dual-purpose, to limit the overall system mass, with solar panels on the backplane providing power for the radar and spacecraft. The proposed solution easily accommodates radar squint angles of +/- 30 degrees for repeat-pass interferometry measurements from multiple directions.

Keywords—Synthetic Aperture Radar, Repeat-pass interferometry, surface deformation, Smallsat

I. INTRODUCTION

Repeat-pass Interferometric SAR [1], also known as InSAR, is by now a well-established tool in the arsenal of Earth scientists, who use it to study surface deformation in geophysically active areas, such as along earthquake faults, in volcanic regions, subsurface aquifers, and the major ice sheets. A long-standing goal of this community [2] has been to field a constellation of InSAR satellites, producing deformation maps in geophysically active areas at up to daily intervals, with full vector displacements at submillimeter per year accuracies. The joint NASA/ISRO SAR mission [3], known as NISAR, and currently planned for launch in 2020, is a significant step on the road to this future capability, with global access on a 12-day revisit interval.

NISAR is a wide-swath (~250 km), medium spatial resolution (~10m) mapping system that provides both L-Band and S-Band InSAR measurements to achieve the mission objectives. Simultaneous wide swath and spatial resolution capability is achieved using the SweepSAR technique [4], a form of scan-on-receive beamforming that uses a large (12m diameter), passive reflector combined with a phased array feed. The requirements expressed in [2] could be met with a constellation of four NISARs, spaced out in separate orbits, according to one of the leading scientists in the Solid Earth science community [5]. The NISAR flight system is a medium to large-class spacecraft, so a 4-element constellation would be very expensive for NASA to undertake on its own – a lower-cost alternative could, therefore, prove to be attractive.

In this paper, we present an architecture for a low-cost S-band InSAR constellation, with a capability that matches a constellation of four NISAR platforms at the same wavelength.

In section II, the factors driving the baseline mission design for the constellation are described. Section III illustrates a novel approach to SAR design, in which the SAR antenna is deliberately sized to be smaller than convention would allow. This builds on work previously published by one of the authors in references [6] and [7]. In section IV we summarize two design approaches for the SAR antenna that are currently under study – a microstrip patch antenna array, and a reflectarray solution. In both cases we expect to populate the backplane of the antenna with solar panels to provide power for radar operations, similar to the ISARA flight demonstration ([8], [9]).

II. MISSION DESIGN

A. Orbit selection

The preferred orbit for the constellation is sun-synchronous, circular and near-polar at an altitude of around 600 km. This orbit provides global access, at the lowest possible altitude for radar operation, with acceptable drag levels to reduce orbit maintenance operations. It is assumed that a constellation of 12 satellites, spaced at one-day intervals, in a 12-day exact repeat orbit, will provide the required temporal revisit frequency.

B. *Launch Strategy*

Specifying an ESPA-ring class spacecraft, with dimensions 1.0x0.7x0.6 m, and mass < 180 kg, allows one to take advantage of low-cost secondary launch opportunities on ESPA ring slots [10]. This enables up to six elements of the InSAR constellation to be launched at a time. After launch, individual elements of the constellation will have to be phased into their required orbits, using a propulsion system, also needed for orbit maintenance. ESPA-ring spacecraft are also compatible with the Venture-class, low-cost small launch vehicles that NASA is currently sponsoring [11], expanding the range of launch options available for the constellation. This flexibility in launch options also makes for easy replenishment of the constellation as it ages and elements are retired.

C. *Spacecraft Selection*

Several spacecraft manufacturers based in the US offer suitably inexpensive, ESPA-ring class spacecraft.

D. *Concept of Operations*

After launch, and orbit phasing, InSAR constellation elements will be uploaded commands for operations spanning up to a week. In the event of, for example, a large magnitude earthquake, commands may be updated more frequently. InSAR data will be collected over geophysically active areas over the land surface. Each element can collect data for up to 30 mins per orbit, allowing coverage over the entire land surface. The nominal orientation for data collection has the radr line-of-sight perpendicular, or broadside, to the orbit track. Vector deformation measurements can be collected at squint angles forward and back from this look direction, requiring a trade-off against temporal coverage. Data will be downlinked at X-band using high-latitude ground receiving stations.

III. RADAR DESIGN

A. *Wavelength selection*

Of the frequencies available for Earth observation using radar, we select S-Band for the following reasons:

- Longer decorrelation times than for shorter wavelengths
- Less severe ionospheric effects than at L-Band
- S-Band SAR antennas are generally smaller than L-Band antennas

B. *Antenna dimensions*

The longest dimension for an ESPA-ring class spacecraft is 1 meter. This sets one dimension of the antenna, which therefore cannot be greater than 1 meter, which determines the antenna height dimension, W. Over typical incidence angles, in the range 25 to 35 degrees, a radar antenna of this height, at an altitude of ~600 km, will illuminate a swath of roughly 80 km in the cross-track direction (assuming broadside pointing). The other dimension, the antenna length L, will be set at the shortest for which reasonable InSAR performance can be achieved. For this study L is set at 5 meters.

C. *Selecting the PRF*

In an earlier paper [6] one of the authors examined the conventional SAR antenna area constraint, showing that it was actually a ‘soft’ constraint, in that SAR systems can be designed and have been operated with antennas smaller than this constraint would normally allow. This design rule in fact only applies when the SAR system engineer seeks to achieve maximum swath width and minimum possible azimuth resolution at the same time.

It follows from [6] that one can design SARs with PRF’s smaller than the Doppler bandwidth provided it is possible to relax the spatial resolution and/or swath width. This result was reported in [7] and is illustrated in Figure 1, in which the Signal-to-Azimuth Ambiguity ratio in dB is plotted for a range of PRF’s smaller than the Doppler bandwidth, against the fraction of the available bandwidth used in processing. In [7] the case when the PRF is set at 70% of the Doppler bandwidth B_D was examined; here the PRF is set at 85% of B_D. Figure 1 shows that reasonable azimuth ambiguity levels < -23 dB can still be obtained if only 40% of the available bandwidth is used in SAR processing (azimuth compression). This means that the best achievable azimuth or along-track resolution is now no longer the well-known L/2 limit of conventional SAR design, but it is degraded by a factor (0.85*0.4)=0.34. For the case where L=5m, the best achievable azimuth resolution is now, therefore, ~7.5m. Note that this still consistent with the NISAR moderate spatial resolution requirement of 10 m.

Two other well-known limits on the PRF from [6] place upper bounds on its value. The first (PRF upper limit 1) says that to avoid significant range ambiguities the PRF must be smaller than the time it takes to collect returns from the *recorded* swath on the ground. The second (PRF upper limit 2) says that the PRF must be smaller than the time it takes to

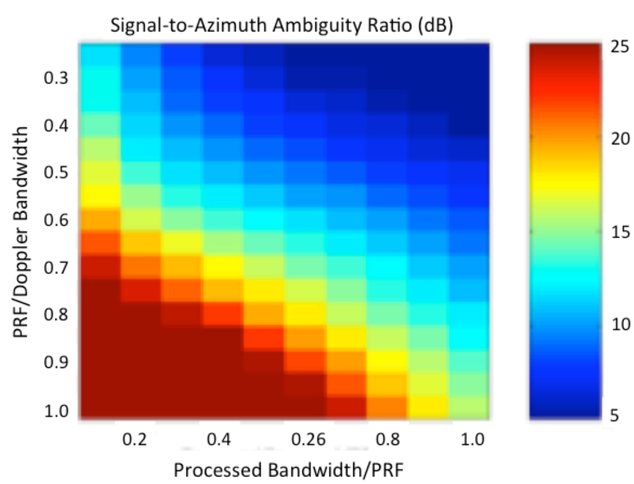

Fig. 1. Signal-to-Azimuth Ambiguity ratios in dB as a function of the PRF expressed as a fraction of the Doppler Bandwidth and the Processed Bandwidth expressed as a fraction of the PRF. Signal and ambiguity levels

were integrated over the available processing bandwidth to generate these results. A planar array with side-looking (broadside) geometry was assumed.

collect returns from the *illuminated* swath on the ground. Generally the recorded swath is smaller than the illuminated swath, so PRF lower limit 2 is more stringent.

Figure 2 shows the PRF upper and lower limits for the S-band case under study, with the PRF selected for nominal broadside operation indicated on the figure. Also shown is the variability of the Doppler bandwidth as a function of squint angle, which was also explored in [7]. Basically, B_D falls off as the antenna is squinted off-broadside. For example, at +/- 30-degree squint angles, this means that the PRF upper and lower limits are much more in line, allowing better azimuth resolution than the broadside case, or more looks in azimuth.

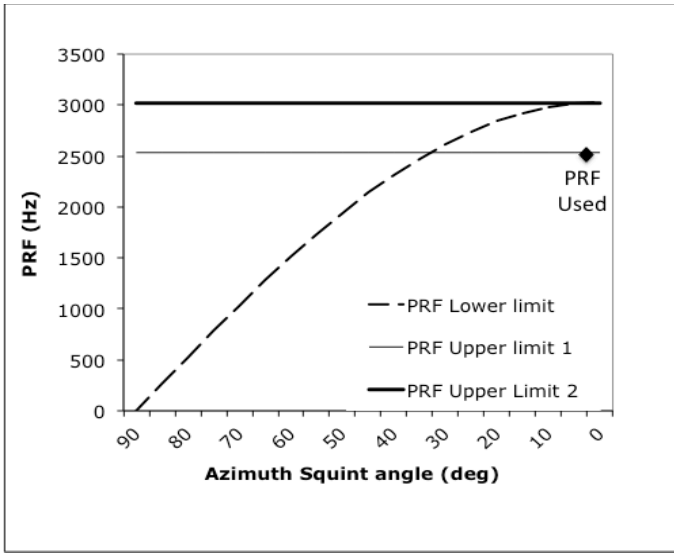

Fig. 2. PRF upper and lower limits for the S-Band SAR example. The PRF value used in the design is indicated. The lower limit on the PRF for a conventional SAR, which depends on the Doppler bandwidth, is shown to vary with squint angle, whereas the two upper limits do not.

TABLE I. S-BAND SAR POINT DESIGN PARAMETERS

Parameter	***Value***
Orbit altitude	600 km
Center frequency	3.2 GHz
Incidence angles	25 – 35 degrees
Squint angle (relative to broadside)	0 degrees
Transmit Peak RF Power	1000 W
DC Power when radar is on	340 W
On-orbit average DC power	102 W
Radar electronics mass	25 kg
Pulse length	50 µs
Antenna dimensions (L X W)	5.0 X 1.0 m
F/D ratio (for reflectarray)	0.5
Bandwidth	25 MHz
Data rate (3:1 presum, 8:4 BFPQ)	65 Mbps
On-time per orbit	20-30 mins
Downlink rate	300 Mbps
Noise-equivalent sigma-zero	-19 dB
Spatial resolution/ (# of looks)	10 m/ (1)
Swath width	80 km

Operating at squint angles +/- 30 degrees off broadside can fulfill the requirement expressed in [3] for vector surface deformation measurements. The trade-offs are that the swath width for off-broadside squint angles will be narrower (by about 30%), and the point spread functions in the SAR image will not be orthogonal. The latter may not matter in SAR data analysis for geophysical applications – the SMAP radar for example was a circular scanning system that obtained higher spatial resolution in the along-track direction using the synthetic aperture technique, at squint angles well off the conventional side-looking, zero-Doppler steered SAR geometry [12]. Point Spread Functions seen in SMAP radiometric data were definitely non-orthogonal. In the case of InSAR the measurement of importance is the relative phase between acquisitions: so conventional SAR image quality is less important.

D. Signal-to-noise

The rest of the SAR design uses the conventional radar equation [13] to define the peak RF power, the transmit pulse length, and the noise-equivalent sigma-zero. An RF amplifier with 40% efficency is assumed in estimating the DC power consumption when the radar is transmitting. This means that 60% of the DC power fed to the radar will actually generate waste heat – it is assumed that this can be dunped to space using a passive radiator. Table II shows the SNR calculation for the noise-equivalent sigma-zero, which is set at -21 dB. – higher levels of backscatter will yield higher SNR.

TABLE II. SNR CALCULATION

Parameter	***dB value***
Peak Transmit Power, P_t	30
Antenna Gain Squared, G_A^2	77.1
Wavelength Cubed, λ^3	-30.8
Speed of light, c	84.8
Pulse length, τ_p	-43
Insertion Loss (2-way)	-8.3
Sigma0	-21
$(4\pi)^3$	33
Range cubed (R^3)	175.5
Boltzmann's constant, k	74
Bandwidth, B	74
Noise Figure	2.5
$2\sin\theta_L$	0.6

SNR	0

E. Data rate

The raw data rate produced by the SAR when operating is also estimated using conventional methods [13], which depend primarily on the bandwidth of the transmitted pulse, B_p and the swath width covered. B_p is set at 25 MHz to provide 10 m ground range resolution at the range of incidence angles adopted for this design. (8:4) bit Block Floating Point Quantization is assumed, and an onboard azimuth prefilter of (3:1) is applied to reduce the data rate to reasonable levels. The azimuth prefilter, applied in the frequency domain, notches out only the one-third of the Doppler bandwidth that is used in azimuth compression.

F. SAR performance

The performance of the S-Band SAR design is summarized in Table I. Note the low on-orbit DC power required to operate the radar, at just 102 W in total, the estimated radar electronics mass of 25 kg, and the low data rate, which is just 65 Mbps. Each of these numbers are sized to fit the power, payload mass and data handling capacity of a typical Smallsat spacecraft platform.

TABLE III.

IV. ANTENNA SOLUTION

The selected antenna architecture is a planar array, deployable in one dimension. It is passive, in that no electronic beam steering or beam forming is required. The required bandwidth is less than 1%, making the design challenge simpler. Table III summarizes the desired characteristics for the SAR antenna.

TABLE IV. DESIRED ANTENNA CHARACTERISTICS

Parameter	*Value*
Antenna dimensions	5×1 m^2
Center frequency	3.2 GHz
Bandwidth	25 MHz
Maximum Possible Boresight Gain	38.5 dB
Flatness requirement after deployment (λ/10)	9 mm

Two approaches for the antenna design are considered: a microstrip patch array, and an offset-fed reflectarray. However, for this study we opted for a microstrip patch antenna array since it does not require the deployment of a feed. Indeed, a 5m × 1m reflectarray antenna would require the deployment of a feed on an extendable boom at a distance of roughly 4m to 5m to achieve a satisfactory efficiency. Figure 3 shows the conceptual design of a 7-panel (5×1m^2) microstrip patch antenna.

The deployable patch array antenna consists of seven 1×0.7m^2 panels made of 14×10 patch elements. The overall conceptual design is illustrated in Figure 4. While the center panel is fixed, three panels are folded on each side of the spacecraft. The side dimension of the spacecraft (i.e. 1×0.7m^2) drives the size of each panel.

The patch elements are entirely made of metal for better thermal stability and efficiency maximization. The radiating elements are 42.5mm-square patches. Each column consists of series-fed microstrip 1×14 patch arrays through air striplines. The 10 columns are fed through a 1×10 corporate feed lines power divider. The 7 panels are then fed through power dividers and cables enabling a 1×7 power distribution.

The cabling and attachments will not take up all of the real estate on the antenna backplane, leaving room for the placement of solar panels. This approach, combining solar array panels and RF antenna, is being flight-tested on the ISARA cubesat ([8], [9]). The antenna designed at 3.2GHz offers a directivity of 38.1dBi. The half power beamwidth equals 4.8 degree in elevation and 1.0 degree in azimuth. We expect a maximum loss of 4.15dB in the two layers of air stripline feeding network and cablings (see Table IV), which has been accounted for in our SNR calculations (Table II).

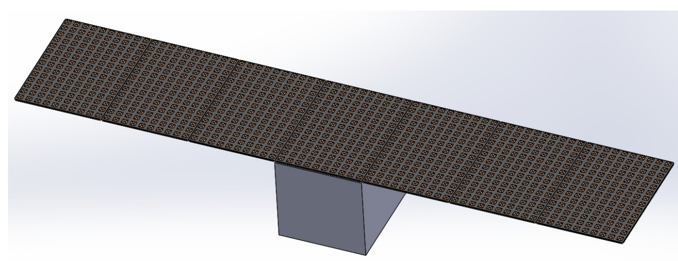

(a)

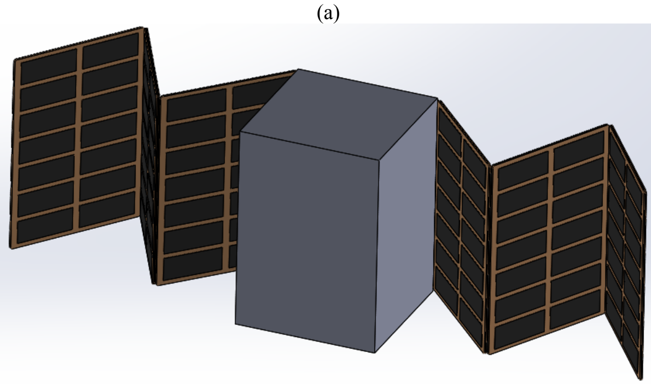

(b)

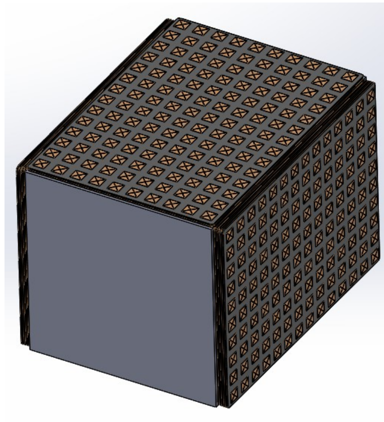

(c)

Fig. 3. S-Band SAR flight system concepts with a deployable microstrip patch array antenna. (a) Deployed. (b) Deploying. (c) Folded.

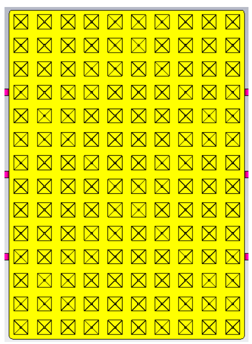

(a)

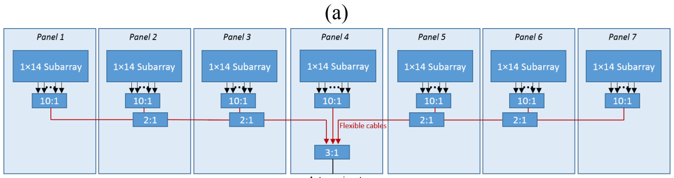

(b)

Fig. 4. Conceptual design for a 7-panel microstrip patch array antenna. (a) Top view of the center panel of the patch array antenna (1m×0.7m). (b) Antenna feeding architecture.

TABLE V. INSERTION LOSS ASSESSMENT

	Loss (dB)
Flexible cables (MCJ311A)	1.2
Power divider	1.25
Air Strip lines	0.6
Connectors	1.1
Total	**4.15**

The antenna radiation pattern is shown in Fig. 5. While the side lobe level (SLL) requirements are very relaxed in elevation, the SLL should be lower than -20dB in azimuth. Hence, a Taylor distribution in employed in the azimuth plane to achieve SLL of -20dB. A gap distance of 20mm to 40mm separates the panels. This gap will be determined by the size of the damped hinge. Calculations have shown that with a gap of 40mm, the antenna performance is not affected. The small effect of this gap is shown in Fig.5b on the SLL.

Deployment tests performed at the NASA's Jet Propulsion Laboratory, using the SMAP's damped hinges, has shown a deployment accuracy of ±0.0005 inches after 7 deployments. This is obviously more than satisfactory at S-band. More effort is planned to further reduce the insertion loss.

V. SUMMARY AND DISCUSSION

A novel architecture for an S-Band InSAR constellation has been presented. Each element of the constellation consists of a simple, single mode of operation, stripmap SAR system, with a passive antenna, mounted on a Smallsat spacecraft bus of modest capability. A 12-satellite constellation following this architecture should be relatively inexpensive to field – roughly equivalent to the cost of a single NISAR flight system, including launch. Such a constellation should satisfy a long-

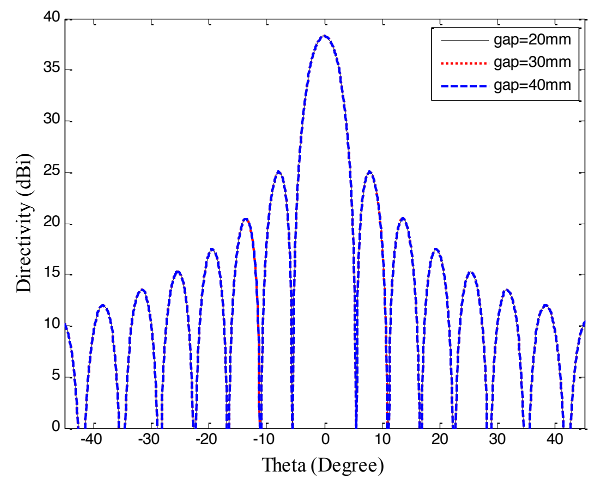

(a)

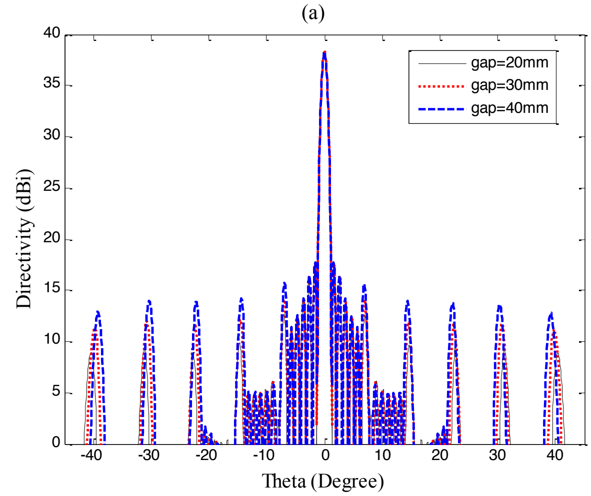

(b)

Fig. 5. Radiation pattern of the 7-panel microstrip patch array antenna for different panel separation ranging from 20mm to 40mm. (a) Elevation. (b) Azimuth.

standing need of the Earth science community for frequent observations of surface deformation phenomena.

The overall performance of the S-Band SAR constellation as an InSAR system measuring surface deformation would depend on the ability of each spacecraft to maintain a precise and repeatable orbit track. In repeat-pass mode [1], InSAR systems require very precise orbit control, especially in the across-track direction, so that each observation is from almost exactly the same vantage point, with little decorrelation. The requirement for NISAR [14] is to fly the same orbit 'tube' for repeat-pass observations, with a maximum allowable separation of 500m in the across-track direction.

The ability to control the orbit of an ESPA-class Smallsat with a SAR antenna deployed, as described here, depends on its drag cross-section, the altitude it operates at, and the capability of its navigation and orbit maintenance systems. DLR's Tandem-X mission team achieved precision flying within a 250 m tube from orbit pass to orbit pass, controlling each satellite's across-track position to within 5m, and along-track to with 50m, at an altitude of 515 km [15]. Both satellites in the Tandem-X pairing use cold gas propulsion for orbit maintenance, and their cross-section in the ram direction is 3.1 m^2 [16]. At the other end of the spacecraft size range, the University of Toronto's 6 kg CanX-4 and CanX-5 nanosats have an areal cross-section of 0.04 m^2. In 2014, they were used to demonstrate autonomous formation flying with sub-meter precision and centimeter-level relative position knowledge, at an altitude of 660 km [17]. This was demonstrated at multiple satellite separation distances, ranging from 50 m to 1000 m. The CanX-4 and -5 satellites both use cold-gas propulsion systems to maintain their orbit position.

The areal cross section of the satellites in the S-Band constellation described here are ~ 0.7 m^2, and the nominal orbit altitude is 600 km, higher than Tandem-X. The S-Band constellation satellites should, therefore, experience less drag than the Tandem-X pair, making orbit maintenance easier. The S-band constellation has a lower altitude than CanX-4 and -5, and a larger area; cross section, so orbit maintenance would be more challenging than for the U. of Toronto demonstration.

From the foregoing we can argue that, while by no means trivial, flying the elements of an S-Band SAR constellation within a 500 m tube to meet the NISAR requirement seems feasible, using a simple cold gas propulsion system for orbit maintenance. Of course, this can only be stated with certainty through a much more in-depth study to define Delta-V required to maintain each satellite in its defined orbit tube over a reasonable mission lifetime.

ACKNOWLEDGMENTS

The research described in this paper was carried out by the Jet Propulsion Laboratory, California Institute of Technology, under a contract with the National Aeronautics and Space Administration. The authors would like to thank our colleagues at Caltech and JPL who stimulated the discussion that led to this architectural solution, including Dr. Charles Elachi, Dr. Paul Rosen, Dr. Mark Simons, Dr. Yunjin Kim, and Jason Hyon; and Dr. Tom Cwik for his support of the antenna design work.

REFERENCES

[1] Rosen, P.A., et al., 2000. Synthetic aperture radar interferometry,Proc. IEEE, Vol. 88, No. 3, March 2000, 333–382.

[2] Living on a Restless Planet, NASA Solid Earth Sceince Working Group, 2002, available at http://solidearth.jpl.nasa.gov/PAGES/report.html

[3] http://nisar.jpl.nasa.gov/

[4] Freeman, A., G. Krieger, P. Rosen, Younis, M., W. T. K. Johnson, Huber, S., R. Jordan, and Moreira, A., SweepSAR: Beam-forming on Receive using a Reflector-Phased Array Feed Combination for Spaceborne SAR, Proc. Radarcon '09, Pasadena, CA, May 2009.

[5] Prof. Mark Simons, Caltech, personal communication, 2016.

[6] A. Freeman, W. T. K. Johnson, B. Honeycutt, R. Jordan, S. Hensley, P. Siqueria, and J. Curlander, "The myth of the minimum SAR antenna area constraint," IEEE Trans. Geosci. Remote Sensing, vol. 38, pp. 320–324, Jan. 2000.

[7] Freeman, A., On Ambiguities in SAR Design, Proc. EUSAR 2006, Dresden, Germany, June 2006.

[8] Hodges, R., Shah, B., Muthulingham, D., and Freeman, A., ISARA – Integrated Solar Array and Reflectarray Mission Overview, Annual AIAA/USU Conference on Small Satellites, August 2013.

[9] R. Hodges, D. Hoppe, M. Radway, and N. Chahat, "Novel deployable reflectarray antennas for CubeSat communications", IEEE MTT-S International Microwave Symposium (IMS), Phoenix, Az, May 2015.

[10] http://www.nasa.gov/press-release/nasa-awards-venture-class-launch-services-contracts-for-cubesat-satellites/

[11] http://www.csaengineering.com/products-services/espa/

[12] West, R., Soil Moisture Active Passive (SMAP) Project Radar Backscatter Calibration for the L1B_S0_LoRes and LIC_S0_HiRes Beta Level Data Products, JPL Document D-93979, available at *https://media.asf.alaska.edu/.../**smap**/*, July 2015.

[13] SAR Systems and Processing, Curlander, J.C. and McDonough, R. N., publ. J. Wiley, 1991.

[14] Rosen, P., personal communication, February 2017

[15] Kahle, R., Schlepp, B., and Kirschner, M., TERRASAR-X / TANDEM-X Formation Control – First Results From Commissioning And Routine Operations, Proceedings of the 22nd International Symposium on Space Flight Dynamics (ISSFD), Feb. 28 - March 4, 2011, Sao Jose dos Campos, SP, Brazil, URL: http://www.issfd22.inpe.br

[16] Krishna, D. M., Improving and Expanding Precision Orbit Derived Atmospheric Densities, M. Sc. Thesis, U. of Kansas, 2012

[17] Bonin, G., et al, Improving and Expanding Precision Orbit Derived Atmospheric Densities, 29th Annual AIAA/USU Conference on Small Satellites, SSC 15-I-4, August 2015.